Experimental investigation on bubble departure diameter in pool boiling under sub-atmospheric pressure

Gao, W.; Qi, J.; Yang, X.; Zhang, J.; Wu, Dawei

DOI:
10.1016/j.ijheatmasstransfer.2019.01.024

Document Version
Peer reviewed version

Citation for published version (Harvard):
Gao, W, Qi, J, Yang, X, Zhang, J & Wu, D 2019, 'Experimental investigation on bubble departure diameter in pool boiling under sub-atmospheric pressure', *International Journal of Heat and Mass Transfer*, vol. 134, pp. 933-947. https://doi.org/10.1016/j.ijheatmasstransfer.2019.01.024

Experimental investigation on bubble departure diameter in pool boiling under sub-atmospheric pressure

Gao, Wenzhong; Qi, Jiaye; Yang, Xuan; Zhang, Jiahao; Wu, Dawei

DOI:
10.1016/j.ijheatmasstransfer.2019.01.024

Document Version
Peer reviewed version

Citation for published version (Harvard):
Gao, W, Qi, J, Yang, X, Zhang, J & Wu, D 2019, 'Experimental investigation on bubble departure diameter in pool boiling under sub-atmospheric pressure', *International Journal of Heat and Mass Transfer*, vol. 134, pp. 933-947. https://doi.org/10.1016/j.ijheatmasstransfer.2019.01.024

Experimental investigation on bubble departure diameter in pool boiling under sub-atmospheric pressure

Wenzhong Gao[1,3], Jiaye Qi[1],Xuan Yang[1], Jiahao Zhang[1], Dawei Wu[2]

(1. Merchant Marine College, Shanghai Maritime University, Shanghai, 201306, China; 2.School of Marine Science and Technology, Newcastle University, Newcastle upon Tyne, NE1 7RU,United Kingdom; College of energy engineering, ZheJiang University, Hangzhou,310058, China)

Abstract

The objective of this research is to compare the nucleate boiling characteristic of the calcium chloride aqueous solution with distilled water at sub-atmospheric pressure by analyzing the growing bubble dynamics in order to provide some data for optimizing the design of the dehumidification system. The experiments were carried out with water and calcium chloride solution on the upper surface of a polished stainless steel plate, under sub-atmospheric pressure ranging from 3.6kPa to 22.0kPa. An artificial nucleation site was created in the center of the plate to generate the isolated bubbles. A high-speed camera was used to capture the images of dynamic bubbles, and the relevant parameters on bubble dynamics were measured and calculated by frame-by-frame image treatment.

Experimental results show that bubble diameter tends to increase with the pressure decrease which means the lower vapor density and stronger surface tension force at sub-atmospheric boiling. The influence of superheat and sub-cooling degree were also analyzed. Additionally, a complex boiling regime of calcium chloride solution with irregular bubble dynamic parameters was observed. Finally, bubble growth dynamics under sub-atmospheric were analyzed and the force balance equation were established. It is shown that the dynamic effect especially the inertial force dominated the growth stage under sub-atmospheric boiling. A new bubble departure diameter correlation within $\pm$20% deviation was proposed.

Keywords: nucleate pool boiling; sub-atmospheric pressure; bubble departure diameter; calcium chloride aqueous solution

Nomenclature

AAD	the average absolute deviation (%)	P_v	the vapor pressure (Pa)
AD	the average deviation (%)	Pr	Prandtl number, Pr = ν/α
Ar	Archimedes number, Ar = $[g\rho_l(\rho_l-\rho_v)/\mu_l^2][\sigma/g(\rho_l-\rho_v)]^{3/2}$	q	heat flux (kW m^{-2})
		R	bubble radius (m)
a	the length of the semi-minor axis (m)	T_{sat}	the saturation temperature(℃)
b	the length of the semi-major axis (m)	T_w	the heated wall temperature(℃)
		T_s	the saturation temperature(℃)
C	a parameter in fritz correlation	t_g	bubble growth period (s)
c_p	specific heat capacity (Jkg)	t_w	bubble waiting period (s)
D_d	bubble departure diameter (mm)	ΔT	surface superheat (K)
D_{eq}	the equivalent bubble diameter (mm)	P_∞	ambient pressure(Pa)
		P_{wall}	the heated wall pressure(Pa)
F_b	buoyancy force (N)		
F_i	inertial force (N)		
F_M	Maragoni force (N)		
F_p	pressure force (N)		
F_s	surface tension force (N)		
f	the bubble departure frequency (Hz)		
g	gravitational acceleration (ms^{-2})		
h_l	the liquid height (cm)	Greek letters	
g_c	gravitational acceleration correction factor	α (m^2s^{-1})	thermal diffusivity
h	the heat transfer coefficient (kW $m^{-1}K^{-1}$)	θ	contact angle, deg
h_{lv}	latent heat (Jkg)	μ	dynamic viscosity (Pa s)
Ja	Jacob number, Ja = $\rho_l c_p \Delta T/\rho_v h_{lv}$	ρ_l	liquid density (kg m^{-3})

K_1	a parameter defined by Jensen and Memmel [20], $K_1 = (Ja/Pr)^2(Ar)^{-1}$	ρ_v	vapor density (kg m^{-3})
L	the calibrated length of the ruler (m)	σ	surface tension coefficient (N m^{-1})
P	pressure (Pa)	ξ	the Maragoni correlation factor

1.Introduction

In recent years, due to new environmental restrictions and ever-increasing demand of energy efficiency, absorption refrigerating plants and liquid desiccant dehumidification systems has become more and more popular. In such systems, nucleate boiling is a widely used method of regeneration due to its high heat transfer coefficient between solid and liquid. Bubble growth and detachment processes have a major impact on nucleate boiling heat transfer. A bubble growth cycle includes: (1)Nucleation period, a bubble nucleates from a single site on the heating surface;(2)Growing period, the bubble grows larger over time, during this period, the convection between liquid and wall is enhanced because of the hot capillary action in vapor-liquid interface;(3)Departure period, when the bubble grows to a certain size, it will depart from the surface, at the same time, liquid with lower temperature will flow into the area that the bubble used to be, so that the wall will be cooled instantly and a lot of heat will be exchanged. It is believed that the nucleation boiling heat transfer is directly influenced by the bubble detachment, so both of the bubble departure diameter and the bubble departure frequency are important parameters that need to be conveyed.

Compared with the boiling heat transfer at atmospheric pressure, it has been found that the boiling heat transfer is deteriorated with lower heat transfer coefficient [1] and larger temperature fluctuations [2-3] at sub-atmospheric pressure. However, only a few studies [2,4-8] on pool boiling at sub-atmospheric pressures have directly characterized bubble formation, growth and dynamic behavior, and developed the correlations for bubble dynamics. The lack of work is partly due to the complexity of the boiling environment at sub-atmospheric pressure. In sub-atmospheric boiling, bubble behavior is quite different from that at the atmospheric conditions. Large non-spherical bubbles, long waiting period, the non-homogeneous boiling environment [5] indicate that traditional models do not apply in the sub-atmospheric conditions. It's also difficult to isolate an individual influencing factor, since the

different phenomenon in sub-atmospheric pool boiling is a result of the combined effects of various factors.

One of the early sub-atmospheric pool boiling experiments was conducted by Yagov et al. [4]. The results of boiling of water, ethyl alcohol and NaCl solution under low pressures were presented. Extremely long period in vapor formation, millimeters-sized bubbles and severe perturbation of the liquid were observed during the experiment. Van Stralen et al. [2] discovered the bubble growth rates of water and organic component at sub-atmospheric pressures. They found that both the bubble growth time and departure radius increase with decreasing pressure. "Rayleigh" bubbles and a high-velocity liquid jet were observed under the low pressure, which was attributed to the occurrence of dry area according to their theory. Giraud et al. [5] pointed out that it was the non-homogeneity environment that results in the different phenomena in the sub-atmospheric pool boiling. The instantaneous boiling curves were presented and a particular "cyclic boiling regime" was investigated in which wall temperature fluctuations can reach 20K. It was also highlighted that the liquid height was an important parameter. Although some typical phenomena were presented and analyzed, those studies remain qualitative. It is still unclear how the theoretical correlations of bubble dynamics obtained under atmospheric condition change under sub-atmospheric conditions. Zajaczkowski et al. [6] analyzed several correlations for heat transfer coefficient in sub-atmospheric conditions, and found the most accurate correlation, but no bubble dynamic parameters were involved. Non-dimensional characteristic radius and time scale parameters were used by Kim et al. [7] to compare the difference between bubble growth behavior at atmospheric and sub-atmospheric pressure. However, the comparison may not be valid because the liquid height was unknown. Michaie et al. [8] used image processing software to calculate some quantitative parameters in sub-atmospheric boiling, but no further analysis was presented. In atmospheric or higher pressure, bubble dynamic parameters and their correlations with influencing factors are studied by numerous researchers. Bubble departure diameter and bubble departure frequency are the crucial parameters referring to bubble dynamics. The correlation proposed by Fritz [9] as shown Eq. (1) has withstood the test of time and were modified by various researchers. The equation was based on pure liquid and liquid mixture, where θ is the contact angle.

$$D_d = 0.0146\theta\sqrt{\frac{2\sigma}{g(\rho_l-\rho_v)}} \quad (1)$$

Cole and Rohsenow [10]have modified the Fritz correlation by involving heat flux appearing in Jacob number.

$$D_d = CJa^{\frac{5}{4}}\left[\frac{2\sigma g_c}{g(\rho_l-\rho_v)}\right]^{\frac{1}{2}} \quad (2)$$

Other mostly used correlations in previous studies are presented in Table 1. All of the correlations were obtained from Mohanty et al. [11]. Those correlations worked well in their experiments, but it is still unknown whether these correlations can predict well under sub-atmospheric boiling conditions.

Table 1

Bubble departure diameter and frequency correlations

$D_d = 0.0208\theta[\frac{\sigma g_c}{g(\rho_l-\rho_v)}]^{1/2}\left[1+0.0025(\frac{dD}{dt})^{\frac{3}{2}}\right]$	Cole and Shulman[12]
$D_d = 0.04Ja[\frac{2\sigma}{g(\rho_l-\rho_v)}]^{1/2}$	Cole[13]
$D_d = 0.25(1+10^5K_1)^{1/2}[\frac{\sigma g_c}{g(\rho_l-\rho_v)}]^{1/2}$	Kutateladeze and Gogonon[14]
For $K_1 < 0.06$, where $K_1 = \left(\frac{Ja}{Pr_l}\right)^2 (Ar)^{-1}$	
$D_d = 0.19(1.8+10^5K_1)^{2/3}[\frac{\sigma}{g(\rho_l-\rho_v)}]^{1/2}$	Jensen and Memmel[15]
$D_d = 0.1649Ja^{0.7}[\frac{\sigma g_c}{g(\rho_l-\rho_v)}]^{1/2}$	Kim and Kim[16]

Though so many researches have been done to investigate bubble departure mechanisms, study about binary mixtures and correlations to predict bubble departure diameter still arises wide interest. In this work, calcium chloride aqueous solution is used as the working fluid to improve our research on dehumidification system regeneration and also to make a thermo-phsical properties comparison with distilled water under the influence of sub-atmospheric pressure. The experiment was conducted on the upper surface of a smooth stainless-steel plate heated by a controlled oil bath. High speed visualization technology was used to monitor the boiling surface, and image processing software was used to extract data. The influence of pressure, superheat, and subcooling degree were presented. Meanwhile, bubble dynamics behavior and force balance were analyzed. Since most of the empirical correlations used in the system design are based on data at atmospheric pressure, by analyzing experimental phenomena, experimental data, and by force analysis, a new correlation suitable for predicting the bubble departure diameter of water and binary mixtures under sub-atmospheric temperature is proposed.

2.Experimental

2.1 Setup

The schematic experimental apparatus of pool boiling are shown in Fig.1. The boiling vessel was constituted by two stainless steel blind plates (diameter 160mm) and a toughened glass cylinder with 90mm inner diameter and 200mm height. They were held together by four bolts and nuts. O-rings seals were placed between the two blind plates and the glass cylinders with the aim of pledging gas-tightness. The vessel was evacuated through a valve connected to a vacuum pump at the top of the upper blind plate. The vapor was condensed through another valve connected to a condenser in order to recycle the evaporated working liquid. Due to the need of frequent assembly and disassembly as well as high gas-tightness, all components of the experimental facilities were made in vacuum technology (ISO-KF).

A stainless steel ruler with the length of 150mm was placed inside the glass cylinder as the reference length to measure the liquid height and bubble size. Two K-type thermocouples were embedded in the upper blind plate and sealed by sealant. They were used to measure the vapor and the liquid temperatures. Another four K-type thermocouples were embedded into the lower blind plate close to the heating surface to evaluate the heat flux with the help of Fourier's law. The calculation of the heat flux and its uncertainty was based on the work of Gong et al. [17]. A fast response thermocouple was placed on the upper surface to measure the instantaneous wall temperature. A pressure transducer with range of 0–20 kPa was used to measure the vapor pressure. Agilent data logger was used to record temperatures, pressures and heat flux. The uncertainties of the measurement instruments are summarized in Table 2.

The experiments were carried out on the upper surface of the lower blind plate. The surface of the stainless steel blind plate was polished with the measured roughness of 0.4μm. An artificial nucleation site with the diameter of 150μm and depth of 70μm [18]was created at the center of the blind plate. The boiling vessel was heated by a controlled oil bath containing silicone oil. During the experiment the oil temperature was set to a constant value in order to maintain a constant given temperature.

A high speed camera was placed near the glass cylinder to capture the pictures of bubbles growth, detachment and breakup. The camera highest acquisition frequency is

1000fps and the resolution is 800×600 pixels. A halogen backlight device was placed in the opposite position to illuminate the boiling area. The 150W halogen lamp can produce intense and homogeneous light to make a decent contrast for clear analysis. The images were analyzed by AOS Imaging Studio software to get the bubble departure diameters. From the captured images, a physical dimension of 90 mm corresponds to 354 pixels, leading to 0.254 mm per pixel. An image processing software was used to measure the contact angle through analyzing the images, as shown in Fig. 2.The contact angle values of water and calcium chloride solution are 35.36 degrees and 32.29 degrees, respectively. As each photo have its own time-stamp, bubble growth period and bubble waiting period can be calculated by finding the creation and detachment frame during a frame-by-frame treatment.

2.2 Determination of the bubble equivalent diameter

Under sub-atmospheric pool boiling conditions, the bubble shape is no longer sphere. In our experiment, a flattened spheroid shaped bubble was observed as shown in Fig. 3a, which is in agreement with Ref [4, 8]. The geometry of a flattened spheroid is shown in Fig. 3b.

As shown in Fig. 3a, the spheroid shape is almost axis-symmetric and a bit non-symmetric in the vertical direction. Therefore, neither of the equatorial diameters 3a nor 3b shown in Fig. 3b can be a good sample of the equivalent diameter. In most previous studies, researchers used the equivalent diameter of a sphere with the same volume. So the bubble equivalent diameter can be calculated as in Eq. (3),

$$D_{eq} = 2\sqrt{ab} \tag{3}$$

2.3 Experimental uncertainty

As mentioned above, the geometry length of bubbles was measured by counting pixels in a captured image. The error of the measurement is of ±2 pixels at the beginning of the growth and ±1 pixels at the end of the growth and the uncertainty of the bubble diameter is ±2.6%.The error of the measurement of contact angle is ±1 degree.

Due to the vacuum environment and good insulation measures, an adiabatic condition can be obtained. According to the Fourier Law, heat flux can be calculated by Eq. (4):

$$q_i = \lambda_i \left(\mathrm{T_i}\text{-}\mathrm{T}_{i-1}\right) / \left(x_i - x_{i-1}\right) \tag{4}$$

Where x_i is the distance between corresponding measurement point and the heating surface, i=1,2,3,4,as shown in Fig. 4;T_i is the temperature,λ_i is the average thermal conductivity of stainless steel between the i-1 point and i point.

The average heat flux is:

$$q = \frac{1}{3}\left\{\sum_{i=1}^{3}\left[\lambda_{i+1}(T_{i+1} - T_i)\left(x_{i+1} - x_i\right)\right]\right\} \tag{5}$$

According to the Taylor experimental error analysis formula, synthetic standard uncertainty (U) is calculated by standard uncertainty (u_i).Since all temperatures are measured by thermocouples whose precision is ± 0.1K,the temperature uncertainty is:

$$u(T) = \sqrt{\left[\frac{\partial(T)}{\partial x_1}u(x_1)\right]^2 + \left[\frac{\partial(T)}{\partial x_2}u(x_2)\right]^2 + \left[\frac{\partial(T)}{\partial x_3}u(x_3)\right]^2} \tag{6}$$

For the length measurement, the standard deviation of ten times length measurements is obtained as:

$$u(\overline{x}_i) = \sqrt{\frac{1}{n(n-1)}\sum_{i=1}^{n}\left(l_i - \overline{l}\right)^2} \tag{7}$$

So the uncertainty of heat flux can be expressed as:

$$u(q) = \sqrt{\begin{aligned}&\left[\frac{\partial f(q)}{\partial T_1}u\left(T_1\right)\right]^2 + \left[\frac{\partial f(q)}{\partial T_2}u\left(T_2\right)\right]^2 + \left[\frac{\partial f(q)}{\partial T_3}u\left(T_3\right)\right]^2 + \left[\frac{\partial f(q)}{\partial T_4}u\left(T_4\right)\right]^2 \\ &+ \left[\frac{\partial f(q)}{\partial l_1}u\left(l_1\right)\right]^2 + \left[\frac{\partial f(q)}{\partial l_2}u\left(l_2\right)\right]^2 + \left[\frac{\partial f(q)}{\partial l_3}u\left(l_3\right)\right]^2 + \left[\frac{\partial f(q)}{\partial l_4}u\left(l_4\right)\right]^2\end{aligned}} \tag{8}$$

2.4 Procedure and operating conditions

Since the experiments need to be implemented under sub-atmospheric pressure, a high level of gas-tightness is required. The entire system, including the condenser and the vacuum pump were cleaned and tested before the experiments. After the test solution was prepared and pipetted into the boiling vessel through a valve, the vacuum

pump was then turned on. When the pressure of the system was stabilized and the dissolved gases were released from the solution, the controlled oil bath was switched on to heat the boiling vessel allowing the saturation temperature of the solution to be reached. Meanwhile, the condenser was turned on to keep the system pressure from rising by condensing the vapor. After the system reached a steady state, the high-speed camera and the halogen lamp were turned on. The visual information as well as the experimental parameters including the surface temperature(P_{wall}), the liquid temperature(ρgh)and the system pressure(P_v) were collected and recorded in a PC-based data acquisition system.

The experiments were conducted with distilled water and calcium chloride aqueous solution. Reagents and distilled water were used to prepare the experimental solution analytically. Distilled water was used in the first set of experiment for eight values of vapor pressure P_v starting from 3.6 kPa up to 22.0 kPa.The liquid height was set as a constant value of $H_l = 15.0\,cm$ for all sets of experiments. The controlled oil bath was set with different oil temperature in each set of experiment to discover the relationship between wall temperature and bubble parameters. Calcium chloride aqueous solution was conducted in the second set of experiments with the same liquid height. Moreover, in order to provide some basic data for future research on promoting the application of low-grade waste heat in solution dehumidification system, five values of vapor pressure P_v starting from 4.2 kPa up to 20.0 kPa were adopted. The full operating conditions and selected physical properties of the experimental solution are presented in Table 3.

3.Results and discussion

3.1 Bubble growth cycle at different sub-atmospheric pressure

3.1.1Boiling environment

Since the experiment was conducted at pressure ranges from 3.6kPa to 22kPa and the working fluids including water and calcium chloride solution, the boiling environment is non-homogeneous mainly due to the following reasons. First, the pressure generated by the liquid height may be in the same order of magnitude as the fluid saturation pressure, which means different liquid height leads to different pressure, as a result, the pressure and saturation temperature of the working fluid can

be highly non-homogeneous[2];Secondly, the different properties of the components in the binary system result in different boiling characteristics, which leads to concentration gradient and temperature gradient starting from the heated surface, the concentration gradient and temperature gradient therefore, strengthen inhomogeneity. Generally speaking, the pressure gradient, concentration gradient and temperature gradient leads to the special boiling environment at sub-atmospheric pressure, as well as the non-homogeneity on bubble growth and shape.

3.1.2Boiling phenomena analysis

In sub-atmospheric pressure, both the bubble size and shape are quite different from those under the atmospheric conditions. The bubble life cycle of distilled water in 4.2 kPa and 22.0kPa is shown in Fig. 5a. As shown in this figure, at $P_v = 4.2$ kPa a bubble nucleates in the artificial nucleation site on the boiling surface and grows with a hemi-sphere shape during the initial 10ms. Then, the bubble is prolonged into a centimeter-sized spheroid shape before detachment. A liquid jet was observed penetrating the lower side of the bubble before the bubble collapses. At $P_v = 20$ kPa, a bubble of the similar shape with the lower pressure was observed, but it was much smaller in size. When the bubble is about to depart, the secondary bubble penetrated the first one and a mushroom shape was observed. The phenomena were similar with those observed by previous studies [2,4,5,8]. According to Van Stralen [2], the high-velocity liquid jet in 4.2kPa is owing to the liquid depression after the primary bubble departs and the formation of the mushroom shape is due to the dry area beneath the center of the first bubble. The author compared this behavior to film boiling because of the low value thermal-conductivity of the vapor.

The bubble growth curves of distilled water at different pressure are shown in Fig. 6a. Take $P_v = 4.2$kPa for example, the initial 40ms can be recognized as the rapid growth period in which the liquid inertia and surface tension force governs. From 40ms to the time that bubble departs, the thermal diffusion dominates the growing process during which bubble grows at slow speed. Comparing the curves at different pressure, it's obvious that with the increase of the pressure level, both the bubble equivalent diameter and bubble growth time decreases. According to Michaie [8], this is because the vapor density ρ_v grows rapidly with the decrease of pressure while the liquid density ρ_l is basically unchanged. Hence, vaporizing certain mass of liquid

require a much larger vapor volume in lower pressure than higher pressure. Surface tension force also increases with the decrease of pressure resulting in the difficulty in the bubble detachment and induces a longer bubble growth time.In general, the analysis mentioned above shows that our experimental method and procedure was verified to be appropriate.

The typical bubble shape of calcium chloride aqueous solution in different pressure is shown in Fig. 5b. Analogously, bubbles of spheroid shape were observed. In lower pressure, large bubbles and high liquid jet were also observed. Owing to the relatively high saturation temperature, there is absence of mushroom bubble in 20kPa which leads to the diminution of the dry area and liquid depression.

The boiling phenomenon of aqueous salt solution can be quite different from the boiling of distilled water based on the following reasons. First, the thermo-physical properties of the salt solution are different from distilled water. The change in saturation pressure, contact angle and surface tension force leads to different boiling characteristics. Secondly, the salt solution belongs to the binary systems, which is different from the pure liquid. During the boiling transfer, the light component in the solution near the heated surface is boiled at first. As the boiling continues, the concentration of the solution near the heated surface is increased, which leads to the change of physical properties near the heated surface.

3.2 Bubble departure diameter and frequency at different sub-atmospheric pressure

3.2.1 Bubble departure diameter and frequency of distilled water

Fig. 6b shows the relationship between bubble departure diameter and pressure of distilled water. It's clear that the bubble departure diameter increases as pressure decreases. At the lowest pressure (P_v =4.2kPa), bubble departure diameter can reach 85mm while at higher pressure (P_v =20kPa) the bubble size is much smaller. As mentioned above, vapor density and surface tension force is the main reason behind this phenomenon. In fact, in most bubble departure diameter correlations, the bubble diameter is proportional to Ja number. As the pressure decreases, vapor density ρ_v increases, which results in the larger size bubble at lower pressure.

The bubble waiting time and frequency at different pressure of distilled water are shown in Fig. 6c. Bubble waiting time is defined as the time interval between the first departing bubbles to the initiation of the successive bubble from the same nucleating

cavity. In the range from 3.6kPa to 22.0kPa, the bubble waiting time decreases from 8s to 0.2s. As a result, bubble departure frequency, defined as the reciprocal of the sum of the bubble waiting time and growth time, increases from 0.1Hz to 4Hz. The long waiting time in the lower pressure conditions is owing to the large size bubbles. The detachment of a bubble of that size leads to strong movement in the surrounding fluid. The liquid near the heating surface is then cooled to approximately the saturation temperature, which need a lot of time to be re-heated to reach the nucleation temperature. As for the mushroom shape(the secondary bubble penetrated the first one) appeared at 20kPa,as shown in Fig. 6e,t_1 is the waiting time between the first bubble and the second one, t_2 is the waiting time between the first bubble and next first bubble, and t_3 is the waiting time between the mushroom and the next mushroom .Considering t_1 is small and the secondary bubble is unstable because it is triggered by the jet flow , so we usually use t_2 as the waiting time, as shown in Fig. 6c.

A comparison between experimental data and literature data was made, as shown in Fig. 7 [3].Considering the difference of working condition and methods, the error of departure diameter at the same pressure is almost within 20%,which means the results of this experiment are accurate.

3.2.2 Comparison with bubble departure diameter and frequency of distilled water and calcium chloride solution

The comparison of the bubble departure diameter and frequency is shown in Fig. 8a. It can be found that the boiling of calcium chloride solution at sub-atmospheric pressure is particularly irregular especially in higher pressure conditions. The irregular departure diameter and frequency reflect the complexity of the boiling conditions of salt solution at sub-atmospheric pressure. In sub-atmospheric pressure, the temperature gradient, pressure gradient and the concentration gradient create a volatile and complex boiling condition. Moreover, the surface tension gradient can be formed by the concentration gradient, which leads to Marangoni flow. The liquid motions caused by preceding bubbles and the size of the previous bubble also have effect on bubble dynamic parameters. This multi-factor combined effect leads to the irregular departure diameter and frequency. Therefore, it is reasonable to compare the overall trend rather than single bubble parameters. Overall speaking, comparing water in the same pressure, the bubble departure diameter of the calcium chloride aqueous solution decreased and the departure frequency increased. Although the increase of the surface

tension force make the bubble harder to detach from the heating surface resulting in longer waiting time and larger bubble diameter. The saturation temperature of the calcium chloride aqueous solution is higher than water in the same pressure, which leads to smaller vapor density. As a result, the bubble departure diameter decreases and the bubble departure frequency increases.

Fig. 8b shows the bubble departure diameter and frequency in different concentration. As shown in Fig. 8b,the irregular distributions still occur in higher concentration. It can be concluded that with the increase of concentration, the bubble departure diameter decreases and the bubble departure frequency increases. The smaller vapor density and stronger Marangoni flow is the reason behind these changes.

3.3 The effect of wall superheat and subcooling degree at sub-atmospheric boiling

Large wall temperature fluctuation was observed during bubbles grew and detach process, which is in agreement with Ref [3, 4, 5]. Therefore, the compared wall superheat is defined in Eq. (5) as

$$\Delta T = T_w(t) - T_{sat}^*, \quad T_S^* = 17.834 \ln P_{wall} - 116.62$$

$$P_{wall} = P_{sat} + \rho g h \tag{9}$$

where $T_w(t)$ is the wall temperature when the nucleation begins and T_s^* is the saturation temperature near the surface. Fig. 9a shows the bubble growth curves in different wall superheat. As the wall superheat rises, both the bubble equivalent diameter and bubble growth time increases, owing to the thicker thermal boundary layer in higher wall superheat [19].

The typical bubble growth curve of saturated boiling and subcooled boiling is shown in Fig. 9b. As shown in the diagram, with the increase of subcooling degree, bubble size decreased which is in agreement with the experimental data of Qiu et al. [20] and the simulation results of Dhir et al. [21]. In saturated boiling, liquid has no need for absorbing heat from bubbles. While in sub-cooled boiling, as shown in Fig. 10, the vapor forming the bubbles re-condenses and release heat. With the increase of the bubble size, the surface area of condensation becomes larger, which results in the

increase of condensation rate. However, due to the limitation of the heat flux, the condensation rate is constrained as well as the bubble size. Therefore, subcooling degree is a constraint on the bubble departure size. Although Marangoni flow that occurs in sub-cooling conditions tends to hinder the departure of the bubbles, considering that the saturated bubble diameter is much larger than that under sub-cooling conditions, the bubble growth period under saturated boiling is still longer than that under sub-cooling conditions at sub-atmosphere.

3.4 A new bubble departure diameters correlation

3.4.1 Comparisons of several correlations for bubble departure diameter

Although the typical bubble shape was observed and the influence with some experimental parameters was summarized, the effects of thermal diffusion, dynamic and non-homogeneous environment in sub-atmospheric pressures still need to be determined. The experimental data was compared with different bubble growth theories and correlations to examine the relative importance of these effects.

One of the foremost bubble growth correlations were proposed by Plesset and Zwick [22] as in Eq. (10). By neglecting the surface tension force and dynamic effects, the bubble growth is only limited by the thermal diffusion process. Accordingly, the solution predicts the instantaneous bubble radius for thermal diffusion dominated growth. The thermal diffusion controlled growth solutions proposed by Plesset and Zwick [22] as well as Forster and Zuber [23] and others are in satisfactory agreement with the experimental data in atmospheric and higher pressures. However, according to Cole and Shulman [12] the heat diffusion limited theory failed to predict the situation under sub-atmospheric conditions. On the other hand, the well-known extended Rayleigh [24] equation as shown in Eq. (11) is based on an equilibrium balance from the dynamic point of view.

$$D=3.908Ja\sqrt{\alpha_l t} \tag{10}$$

$$\frac{P_v(T_v)-P_\infty}{\rho_l}=R\frac{d^2R}{dt^2}+\frac{3}{2}\left(\frac{dR}{dt}\right)^2+\frac{2\sigma}{\rho_l} \tag{11}$$

As is illustrated in Fig. 11, when the pressure was about 20kPa and the Jakob number approximately equaled to 267, the theoretical curves lay above the experimental data. With the pressure being reduced to 7.3kPa and the Jakob number

388 equaled to 662, the deviation of the Plesset and Zwick correlation became larger. In
389 the lowest pressure 4.2kPa and the highest Jacob number 1786, the experimental data
390 in the early growing stage coincided with the Rayleigh curves, while the Plesset and
391 Zwick correlation didn't predict well in this situation. These comparisons indicate that
392 the early growth stage of bubble growth process under sub-atmospheric pressures is a
393 significant inertia controlled region.

394 **3.4.2 The force balance of the bubble under sub-atmospheric pressure**

395 In order to discover the dynamic behavior and obtain a useful bubble growth model
396 under sub-atmospheric pressure, it's important to identify which of the acting forces
397 are dominant. The force balance of the isolated bubble is presented in this chapter to
398 further analyze the influences of each force under sub-atmospheric pressure. As is
399 mentioned above, the flattened spheroid shape is the typical shape of an isolated
400 bubble under sub-atmospheric boiling conditions. The geometric parameters and force
401 analysis of an isolated bubble is shown in Fig. 12a.

402 Generally speaking, buoyancy force F_b and pressure force F_p are the positive
403 forces are those tend to push the vapor bubble on to the heating surface. While the
404 drag force F_d , surface tension force F_s , the Marangoni force F_M and inertial force F_i
405 are the negative forces that prevent bubbles from departing from the heating surface.
406 As a result, the expression of forcer balance is presented in Eq.(12):

407 $$F_b + F_p = F_M + F_s + F_i + F_d \tag{12}$$

408 The expressions of each force are:

409 1. Buoyancy force F_b is caused by the movement of the fluid due the non-uniform
410 density.

411 $$F_b = \frac{4}{3}\pi R_{eq}^3 g\left(\rho_l - \rho_v\right) \tag{13}$$

412 2. Pressure force F_p is the contact capillary pressure force caused by the surface
413 tension in the solid-liquid interface.

414 $$F_p = \pi R_c^2 \frac{2\sigma}{R_{eq}} \tag{14}$$

3. The inertial force F_i is deduced by the velocity of the bubble and the volume expansion.

$$F_i = \frac{d}{dt}(m_l v) \tag{15}$$

4. The Maragoni force F_M is caused by surface tension gradient in the vapor-liquid interface. In atmospheric conditions the surface tension gradient is mainly caused by temperature gradient. However, in sub-atmospheric conditions the pressure gradient should not be neglected.

$$F_M = \xi_t \frac{d\sigma}{dt}\Delta T + \xi_p \frac{d\sigma}{dt}\Delta p \tag{16}$$

5. The surface tension force F_s acts on the vapor-liquid interface is shown in Eq.15

$$F_s = 2\pi R_c \sigma \sin\theta \tag{17}$$

The relationship between the forces acting on the isolated bubble and the bubble radius was presented in Fig. 12b and Fig 12c. As can be seen from the curves, in sub-atmospheric boiling conditions, the buoyancy force F_b and inertial force F_i are obviously the dominant forces. Due to the low vapor density in lower pressure, the large volume of bubbles leads to the exponential growth of the buoyancy and inertial force compared to the situation in atmospheric pressures. On the other hand, the influence of the other three forces is relatively small and can be neglected in the sub-atmospheric pressure. The curves also concurs with the comparison result in the previous chapter that the inertial forces are the major factor that hinders the bubble detachment.

The results also indicate that the bubble departure diameter correlations such as Fritz correlations based on the static force balance of the buoyancy and surface tension force may not be valid under sub-atmospheric pressure. Considering the significant inertia controlled region, an attempt should be made to find a new correlation in the sub-atmospheric pool boiling conditions.

3.4.3 New corrlation

As is mentioned above, in sub-atmospheric pressures, the initial force is the dominant negative force. As a result, the force balance equation can be written below,

$$g\left(\rho_l-\rho_v\right)V\left(t_g\right)=\frac{d}{dt_g}\left(m_l v\right) \tag{18}$$

where $V\left(\mathrm{t}_g\right)$ is the volume of the bubble.

Assume that the equivalent bubble diameter $D_{eq}\propto t_g^n$, $\rho_v << \rho_l$ and $v=\frac{dh}{dt_g}$, the Eq.18 can be rewritten as:

$$\frac{d}{dt_g}\left(t_g{}^{3n}\frac{dh}{dt_g}\right)=gt_g{}^{3n} \tag{19}$$

Therefore, the $h(t_g)$ can be written as:

$$h(t_g)=\frac{gt_g{}^2}{6n+2} \tag{20}$$

At the moment of a bubble's detachment, as is shown in Fig. 13, the bubble is a flattened spheroid shaped and the $h(\tau_d)$ can be written in this form:

$$h(t_g)=b \tag{21}$$

By analyzing the experimental data, it can be found that the ratio of minor axis and the major axis is approximately a constant value $b/a=0.3$. Therefore, Eq.(21) can be rewritten as:

$$h(t_g)=\frac{\sqrt{30}}{10}R_{eq} \tag{22}$$

Kim et al[11] pointed out that the bubble radius is proportional to the power of 2/3-1/2 of growth time. According to our experimental data, the parameter n is equal to 1/2. So the bubble departure diameter is:

$$D_d=\frac{2\sqrt{30}}{15}gt_g^2 \tag{23}$$

3.4.4 Comparison of bubble departure diameters correlations with experimental data

The six most commonly used bubble departure diameters correlations were chosen to compare with the experimental data. As defined in Eq. 24 and 25, the average deviation (AD) and the absolute average deviation (AAD) are used to evaluate those correlations. The results are presented in Table 4 and the comparisons between the experimental and predicted bubble diameters are shown in Fig. 14.

$$AD=\frac{1}{N}\sum_{1}^{N}\frac{predictedvalue\text{-}exprimentalvalue}{exprimentalvalue}\times 100 \quad (24)$$

$$ADD=\frac{1}{N}\sum_{1}^{N}\left|\frac{predictedvalue\text{-}exprimentalvalue}{exprimentalvalue}\right|\times 100 \quad (25)$$

As is presented in Table 4, Fritz [9] and Cole and Shulman [12] didn't predict well in sub-atmospheric pressure, with deviations more than 95% in all of the conditions. Cole and Shulman [12] include the bubble growth rate based on Fritz correlation. However, due to lack of Jacob number in their correlations, the effect of the system pressure is neglected. As a result, their correlations are limited in sub-atmospheric conditions. Cole [13] modified Fritz correlation by taking a constant number 0.04 instead of the contact angle and involving the Jacob number. The data show the trends and work reasonably in 20kPa, but in lower pressure large deviations are observed.

By integrating three dimensionless numbers Ja , Pr and Ar into K_1 , the correlations proposed by Kuyayeladze and Gogonin [14] and Jensen and Memmel [15] were quite similar. The correlation developed by Jensen and Memmel [15] showed big deviations in all of the conditions except for 12.3kPa. Kuyayeladze and Gogonin [14] agreed well within $\pm 30\%$ at three conditions (20kPa water, 7.2kPa water and 7.2kPa $CaCl_2$ solution). However, in lower pressure (5.6kPa), their correlation was not applicable because the dimensionless number K_1 got out of range ($K_1 > 0.06$). The correlations proposed by Kim and Kim [16] showed the best results with deviations with $\pm 30\%$ in all of the conditions. Dimensional analysis involving the characteristic time scale and characteristic bubble radius scale were used in their studies.

The comparison between the experimental and Eq.19 is illustrated in Fig. 15a. As can be seen from the picture, the new correlation predicted well in all of the experimental conditions. The predicted departure diameters of the new correlation were within $\pm 20\%$ deviation, which showed great improvement to predict in sub-atmospheric pool boiling conditions.

3.4.5 Comparison of new bubble departure diameter correlation with different literature data

In this section, a comparison between literature data [2][25][26]and prediction data that calculated by new correlation was made. Stralen and Cole [2] took water as working fluid, the working pressure ranges from 4.08kPa to 20.28kPa.While Stralen, Sluyter and Cole [25] took water, water-ethanol and water-1-butanol as working fluid, the pressure ranges from 3.6kPa to 6.6kPa.The working fluid of Cole and Shulman's [26] experiment was water, the pressure was between 6.7kPa and 13kPa.As shown in Fig. 15b, the new correlation predicts well in most of the experimental conditions, especially for water(4.08kPa)[2,26] and binary mixtures (3.6kPa-6.6kPa)[26].

4. Conclusions

Nucleate pool boiling experiments of water and calcium chloride solution were carried out at sub-atmospheric pressure in a range of 3.6kPa to 22.0kPa. A high-speed camera was used to capture the bubble images. The bubble dynamic parameters were measured and calculated, the bubble growth curves in different boiling conditions were obtained. The main conclusions are listed as follows.

For distilled water, due to the low vapor density and high surface tension force, the bubble diameter tends to increase as pressure decreases. Additionally, as the wall superheat rises, the thermal boundary layer become thicker and results in larger bubble departure diameters. In sub-cooling conditions, the condensation effect and the Marangoni flow hinder the bubble growth, resulting in a smaller bubble size. The experiments of water verified the methods and procedure successfully, and provide basic data for the new correlation.

For calcium chloride solution, a complex boiling regime with irregular bubble dynamic parameters was observed ,comparing to water under the same pressure, the effect of smaller vapor density outweighs that of the surface tension force, which results in the decrease in departure frequency and increase in departure diameter. Moreover, with the increase of concentration, the bubble departure diameter tends to decrease and frequency tends to increase respectively owing to the smaller vapor density and stronger Marangoni flow.

Finally, based on bubble force balance analysis, the relationship of buoyancy force, pressure force, the inertial force, the Maragoni force and the surface tension force was analyzed. Considering sub-atmospheric pressure environment, the inertia force is the dominant negative force, so after simplification of force balance equation, a new

529 correlation was proposed. The developed correlation can predict the whole data of
530 distilled water and calcium chloride solution within ±20% deviation. For the
531 literature data, the developed correlation has a mean deviation of 17.2% and 6.3% for
532 water and binary mixtures, respectively.

533

534 **Acknowledgments**

535 The research work described in this manuscript was supported by the National
536 Natural Science Foundation of China (Grant No.51106094) as well as Natural Science
537 Foundation of Shanghai (Grant No. 16ZR1414700 and 18040501800). Their support
538 is gratefully acknowledged.

539

540 Reference

[1] R. McGillis, V.P. Carey, J.S. Fitch, W.R. Hamburgen, Pool boiling on a small heat dissipating element in water at low pressure, in: ASME/AIChE National Heat Transfer Conference, Minneapolis, Minnesota, 1991.

[2] S.J.D. van Stralen, R. Cole, W.M. Sluyter, M.S. Sohal, Bubble growth rates in nucleate boiling of water at sub-atmospheric pressures, In International Journal of Heat and Mass Transfer, Volume 18, Issue 5, 1975, Pages 655-669, ISSN 0017-9310

[3] S.J.D. Van Stralen, W.M. Sluyter, Local temperature fluctuations in saturated pool boiling of pure liquids and binary mixtures, In International Journal of Heat and Mass Transfer, Volume 12, Issue 2, 1969, Pages 187-198, ISSN 0017-9310.

[4] V.V. Yagov, A.K. Gorodov, D.A. Labuntsov, Experimental study of heat transfer in the boiling of liquids at low pressures under conditions of free motion, J. Eng. Phys. 18 (1970) 421–425.

[5] Florine Giraud, Romuald Rullière, Cyril Toublanc, Marc Clausse, Jocelyn Bonjour, Experimental evidence of a new regime for boiling of water at subatmospheric pressure, In Experimental Thermal and Fluid Science, Volume 60, 2015, Pages 45-53, ISSN 0894-1777.

[6] B. Zajaczkowski, T. Halon, Z. Krolicki, Experimental verification of heat transfer coefficient for nucleate boiling at sub-atmospheric pressure and small heat fluxes, Heat Mass Transf. 52 (2016) 205–215.

[7] Jeongbae Kim, Cheol Huh, Moo Hwan Kim, On the growth behavior of bubbles during saturated nucleate pool boiling at sub-atmospheric pressure, In International Journal of Heat and Mass Transfer, Volume 50, Issues 17–18, 2007, Pages 3695-3699, ISSN 0017-9310.

[8] Sandra Michaie, Romuald Rullière, Jocelyn Bonjour, Experimental study of bubble dynamics of isolated bubbles in water pool boiling at subatmospheric pressures, In Experimental Thermal and Fluid Science, Volume 87, 2017, Pages 117-128, ISSN 0894-1777.

[9] Fritz W. Maximum volume of vapor bubbles. Phys Z. 1935;36:379–84.

[10] Cole R, Rohsenow WM. Correlation of bubble departure diameters for boiling of saturated liquids. Chem Eng Prog Symp Ser 1969;65(92):211–3.

[11] Rajiva Lochan Mohanty, Mihir Kumar Das, A critical review on bubble dynamics parameters influencing boiling heat transfer, In Renewable and Sustainable Energy Reviews, Volume 78, 2017, Pages 466-494, ISSN 1364-0321, https://doi.org/10.1016/j.rser.2017.04.092.

[12] Cole R, Shulman HL. Bubble departure diameters at sub-atmospheric pressures. AIChE Chem Symp Ser 1966;62(64):6–16.

[13] Cole R. Bubble frequency and departure volumes at sub-atmospheric pressures. AIChE J 1967;13:779–83.

[14] SS. Kutateladze, II. Gogonin, Growth rate and detachment diameter of a vapor bubble in free convection boiling of a saturated liquid,TeplofizikaVysokikhTemperatur 17 (1979) 792–797.

[15] M.K. Jensen, G.J. Memmel, Evaluation of bubble departure diameter correlations, in: Proceedings of the Eighth International Heat Transfer Conference, vol. 4, 1986, pp. 1907–1912.

[16] J. Kim, M.H. Kim, On the departure behaviors of bubble at nucleate pool boiling, Int. J. Multiph. Flow 32 (10) (2006) 1269–1286.

[17] M. Gong, J. Ma, J. Wu, Y. Zhang, Z. Sun, Y. Zhou, Nucleate pool boiling of liquid methane and its natural gas mixtures, Int. J. Heat Mass Transf. 52 (11) (2009) 2733–2739.

[18] John R. Howell and Robert Siegel,Incipience,growth, and detachment of boilingbubbles in saturated water from artificial nucleation site of known geometry and size. Technical paper proposed for presentation at Third International Heat Transfer Conference Chicago, Illinois, August 8- 12, 1966.

[19] Zuber N, Hydrodynamics aspects of boiling heat transfer, US AEC Report AECU 4439, 1959.

[20] Qiu DM, Dhir VK, Hasan MM, Chao D, Neumann E, Yee G, Witherow J. Single Bubble Dynamics during Nucleate Boiling under Microgravity Conditions. Engineering foundation Conference on microgravity fluid physics and heat transfer. Honolulu, HI; 1999.

[21] Dhir VK, Abarajith HS, Li D. Bubble dynamics and heat transfer during pool and flow boiling. Heat Transf Eng 2007;28(7):608–24.

[22] M.S. Plesset, S.A. Zwick, The growth of vapor bubbles in superheated liquid, J. Appl. Phys. 25 (1954) 493–500.

[23] H.K. Forster, N. Zuber, Growth of vapor bubbles in superheated liquid, J. Appl. Phys. 25 (1954) 474–478.

[24] J. Kim, M.H. Kim, On the departure behaviors of bubble at nucleate pool boiling, Int. J. Multiph. Flow 32 (10) (2006) 1269–1286.

[25]S.J.D. Van Stralen, W.M. Sluyter and R.Cole,Bubble growth rates in nucleate boiling of aqueous binary systems at sub-atmospheric pressures , Int. J.Heat Mass Transfer. 1975:19:931-941.

[26] Cole R, Shulman HL, Bubble growth rates at high jakob numbers, Int. J. Heat Mass Transfer. 1966:9:1377-1390.

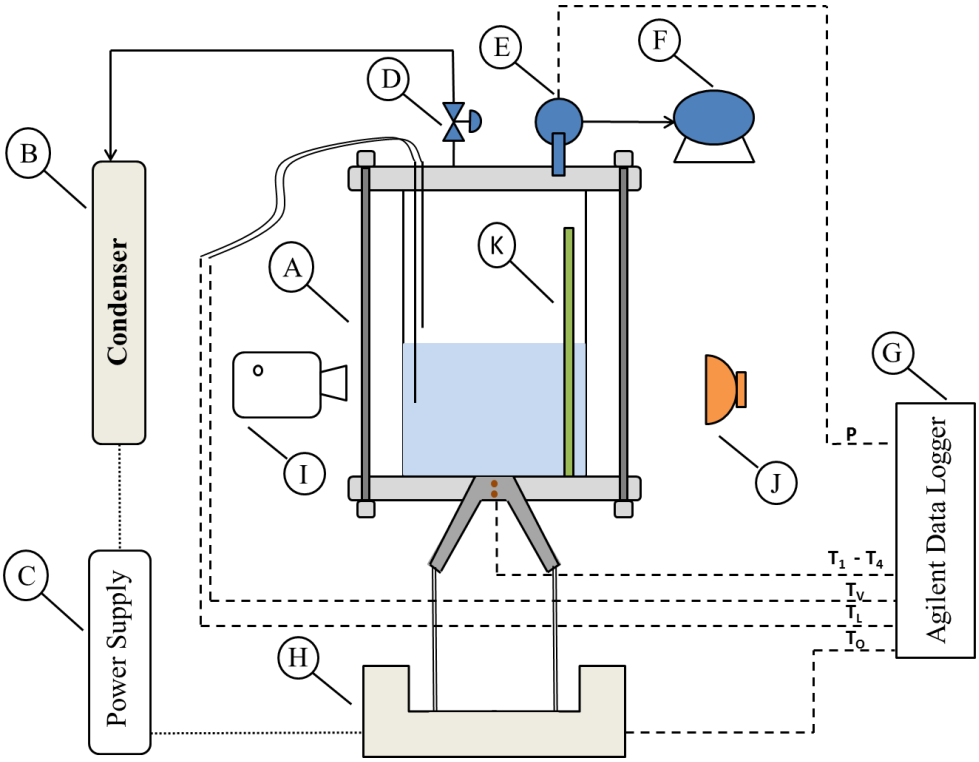

Figure.1. Schematic of the experimental apparatuses. (A) Boiling Vessel; (B) Condenser; (C) Power Supply; (D) Valve; (E) Vacuum Pressure Transducer; (F) Vacuum Pump; (G) Agilent Data Logger; (H) Controlled Oil Bath; (I) High Speed Camera; (J) Halogen Backlight Device; (K) Stainless Steel Ruler

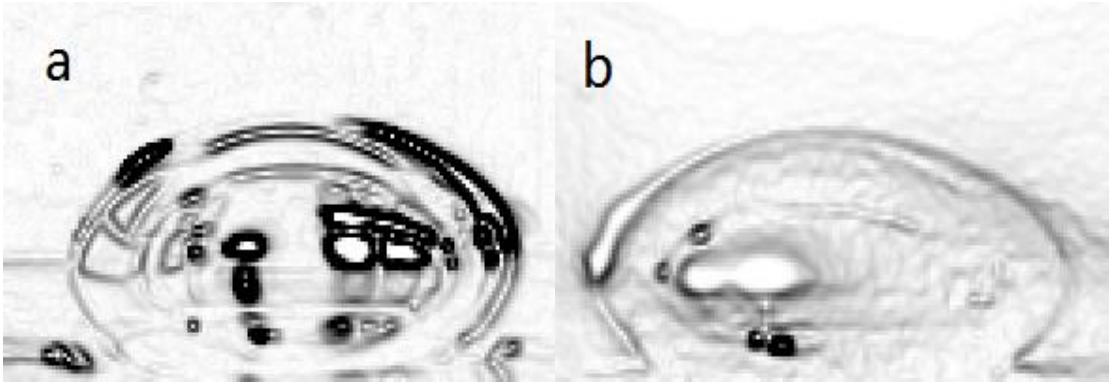

Fig. 2. Processed bubble images of distilled water(a) and calcium chloride aqueous solution(b)

(P_v =20kPa,H_1 =15cm,T_s =60℃)

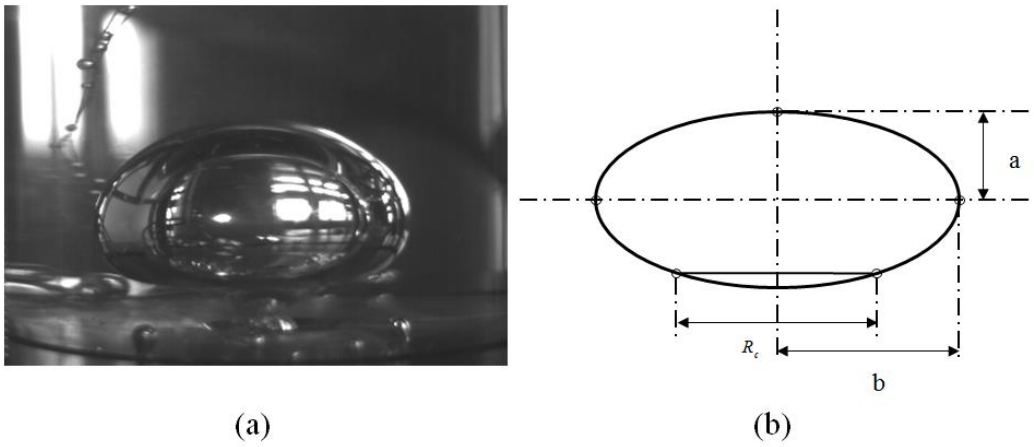

Figure.3 A flattened spheroid shaped bubble (a) and the geometry of a flattened spheroid(b)

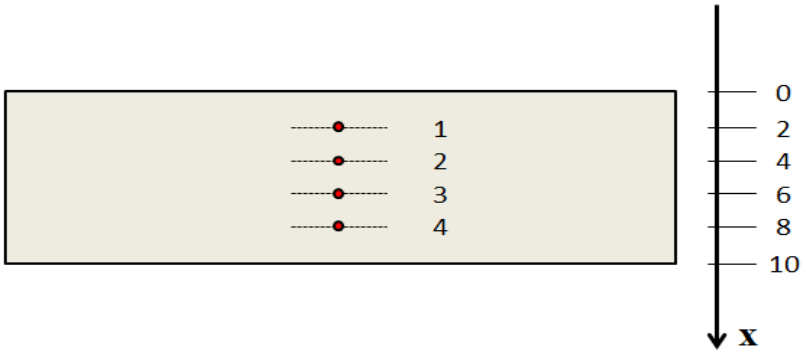

Fig. 4 . Corresponding measurement points schematic diagram

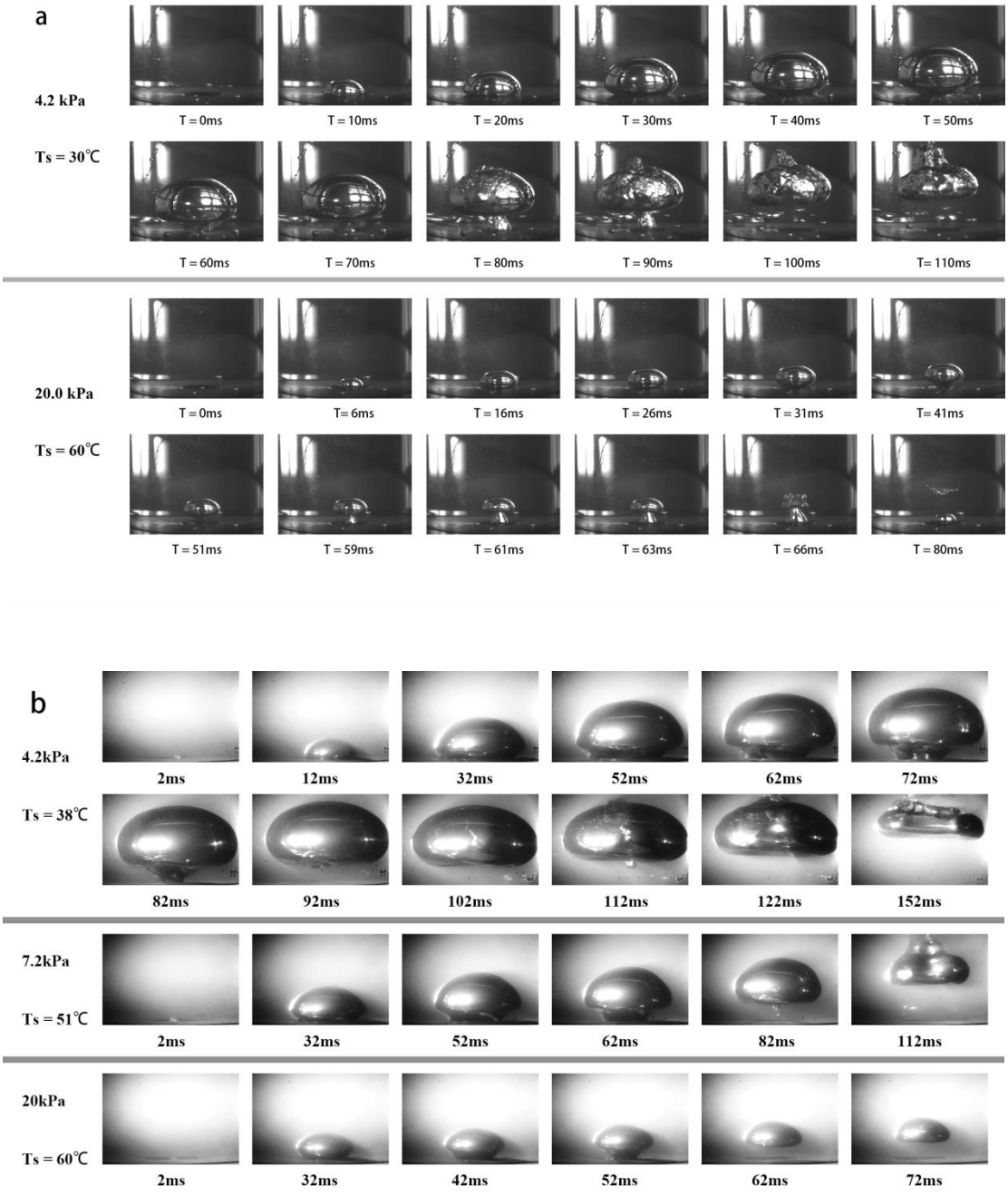

Figure.5. Typical Bubble shape under different pressure (a)(dstilled Water, $H_l = 15cm, \Delta T = 20K$) ,(b) (calcium chloride aqueous solution , $H_l = 15cm, \Delta T = 20K, wt = 30\%$)

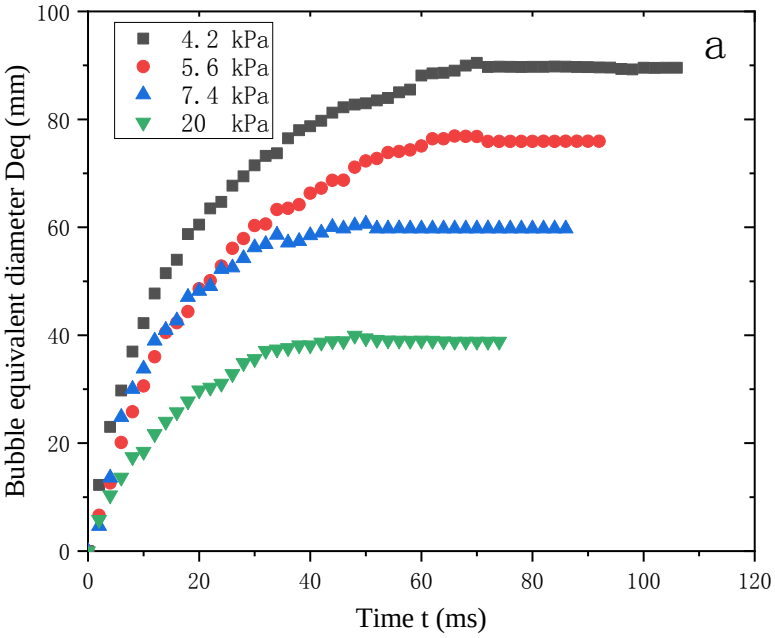
a
4.2 kPa
5.6 kPa
7.4 kPa
20 kPa
Bubble equivalent diameter Deq (mm)
Time t (ms)
0
20
40
60
80
100
120

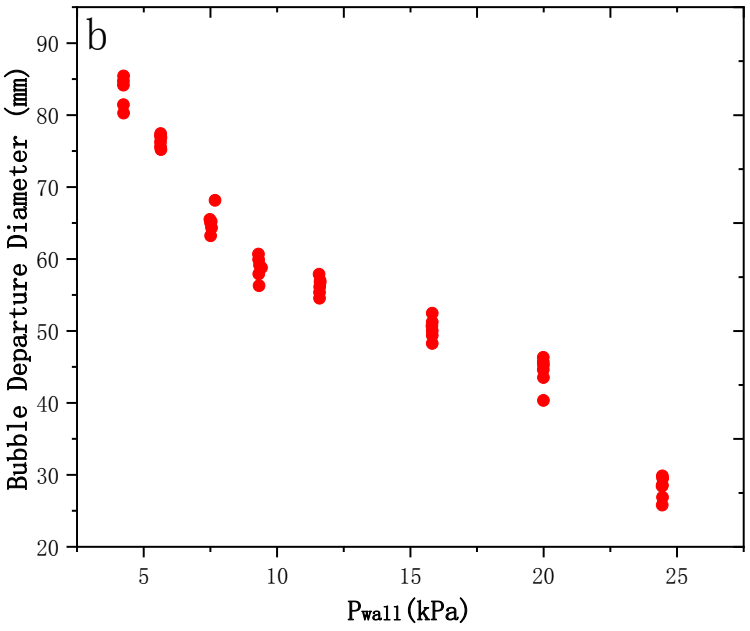
b
Bubble Departure Diameter (mm)
Pwall (kPa)
20
30
40
50
60
70
80
90
5
10
15
20
25

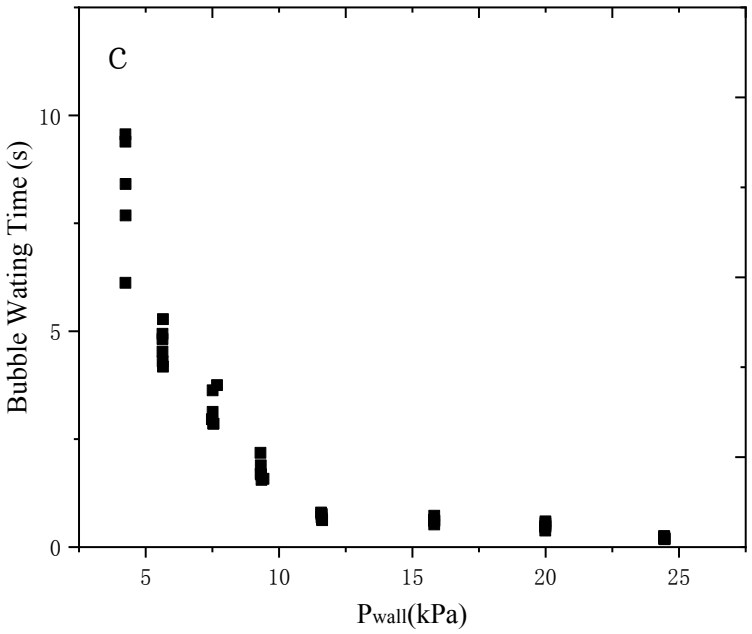
c
Bubble Wating Time (s)
0
5
10
5
10
15
20
25
Pwall(kPa)

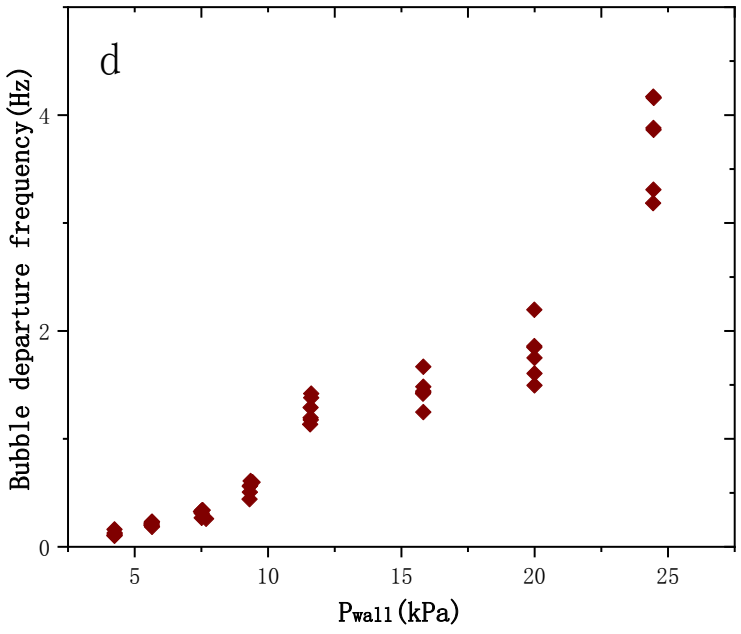
d
Bubble departure frequency (Hz)
0
2
4
5
10
15
20
25
Pwall (kPa)

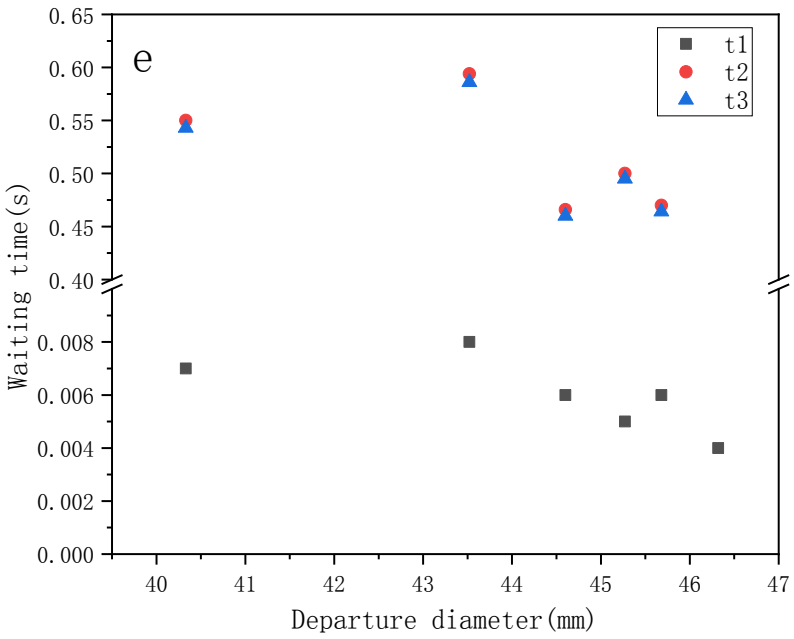

$$(\text{Distilled Water}, H_1 = 15\text{cm}, \Delta T = 40\text{K}, \Delta T_{sub} = 0\text{K})$$

Figure.6.Bubble growth curves(a),bubble departure diameter(b),bubble waiting time(c) and departure frequency(d) at different pressure and bubble waiting time of mushroom shape bubble at 20kPa(e).

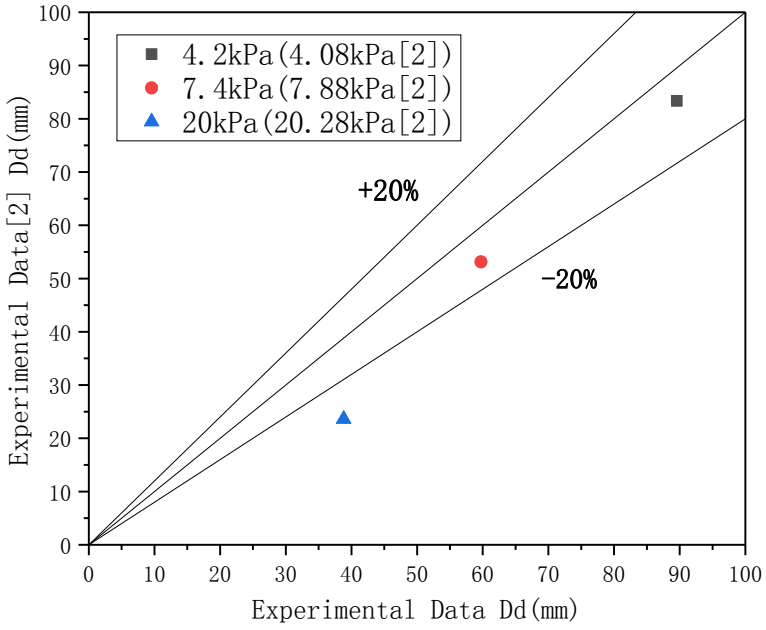

Figure.7. Experimental bubble departure diameter in comparison with literature data[2]

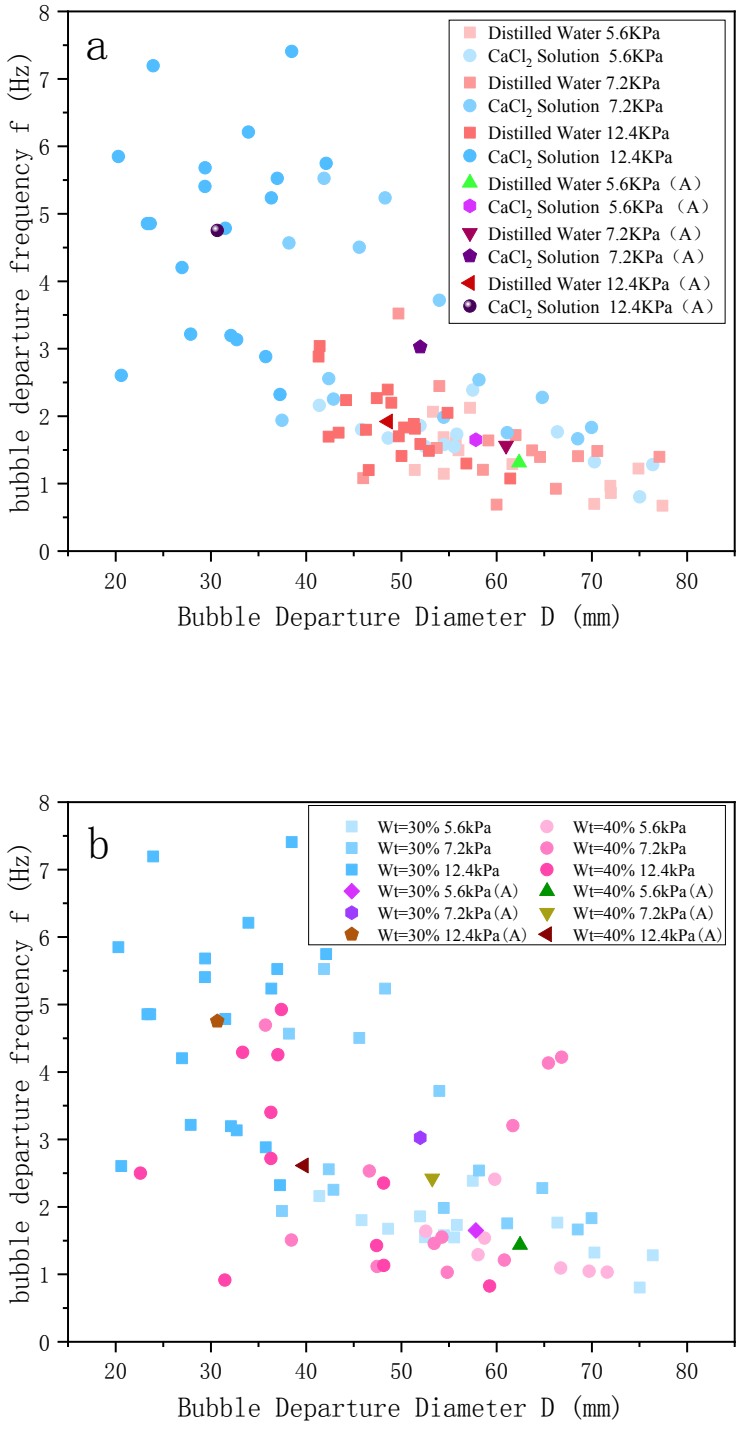

Figure.8. The comparison between distilled water and calcium chloride aqueous solution of bubble departure diameter and frequency in different pressure(A:Average value)($H_1 = 15\text{cm}, \Delta T = 20\text{K}, \text{wt} = 30\%$)(a) and the bubble departure diameter and frequency in different concentration(A:Average value)(calcium chloride aqueous solution, $H_1 = 15\text{cm}, \Delta T = 20\text{K}$)(b)

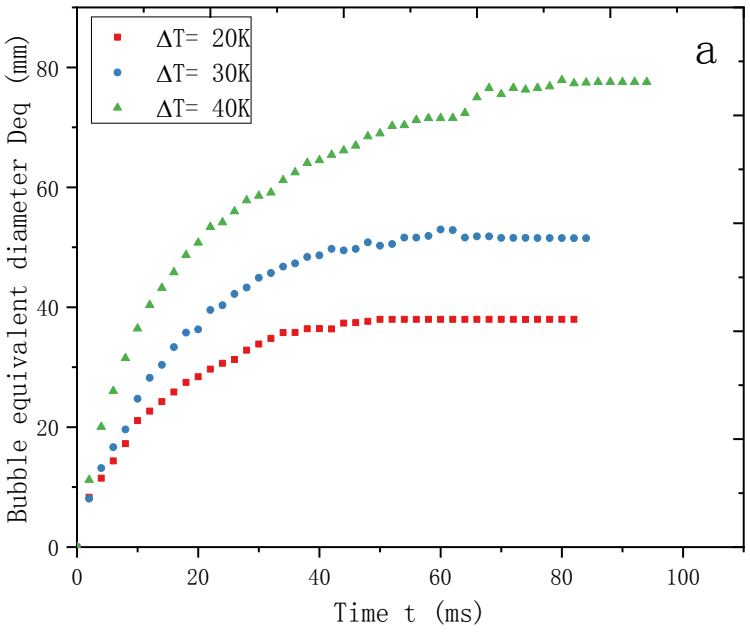

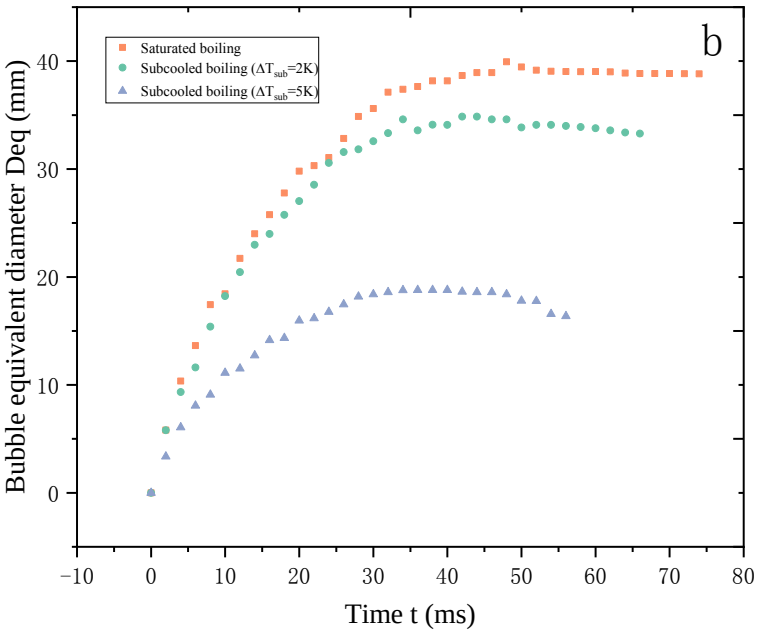

Figure.9. The bubble growth curves under different values of superheat temperature(Distilled Water, $P = 5.6\text{kPa}, H_1 = 15\text{cm}$)(a) and the bubble growth curves in saturated boiling and subcooled boiling(Distilled Water, $P = 20\text{kPa}, H_1 = 15\text{cm}, \Delta T = 30\text{K}$)(b)

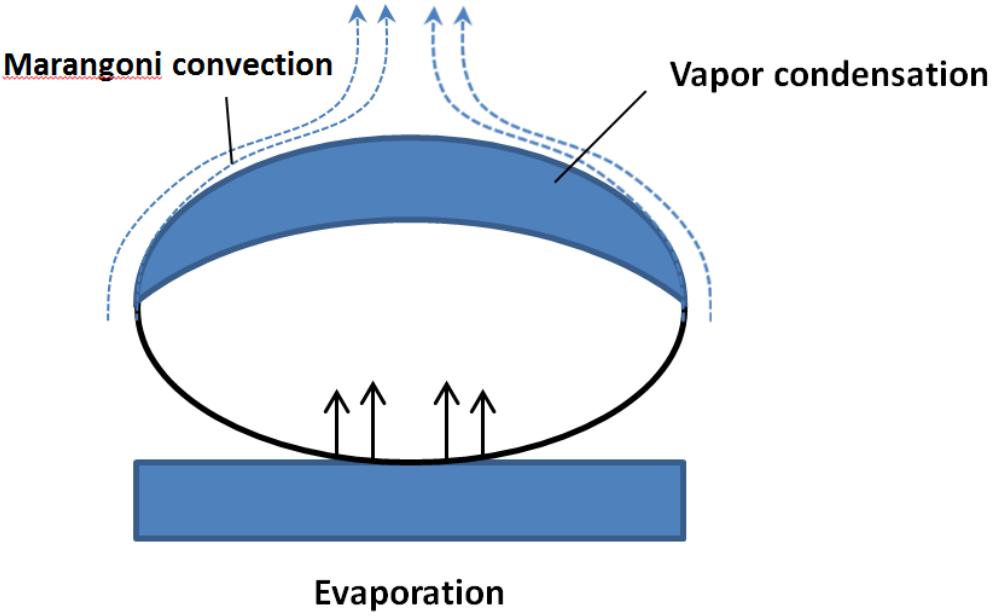

Figure.10. The subcooled boiling mechanism

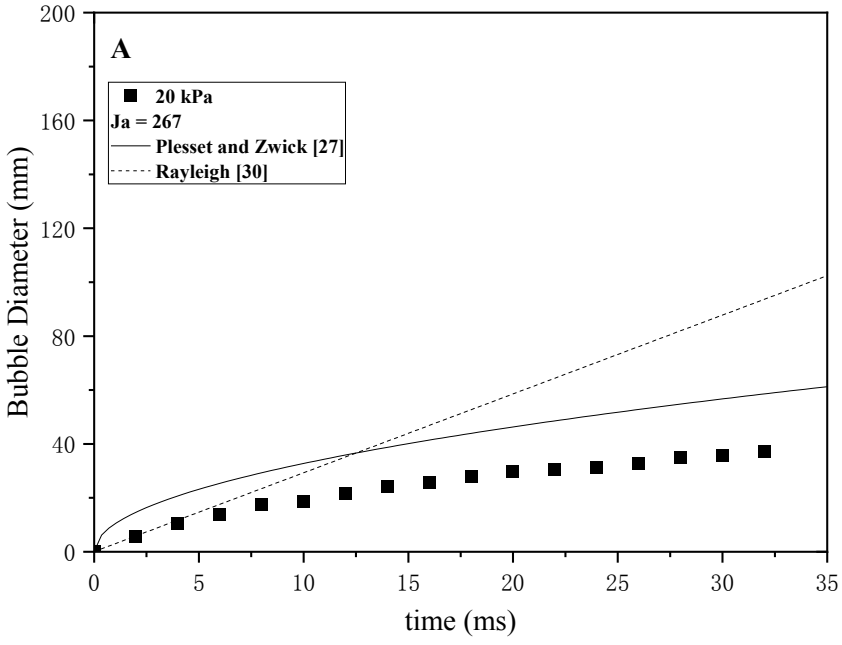

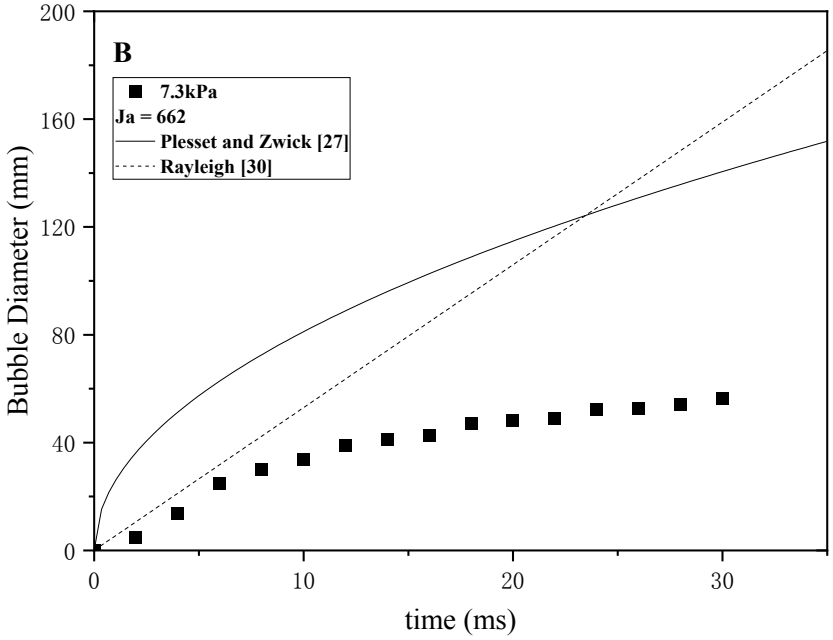

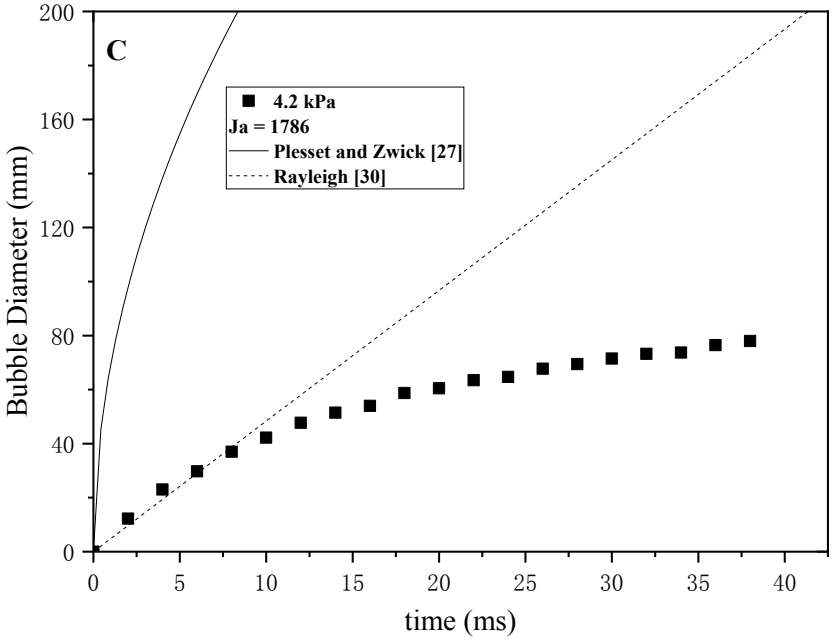

Figure.11. Comparison of the growth rate correlations with experimental data

(Distilled Water, $H_l = 15cm$)

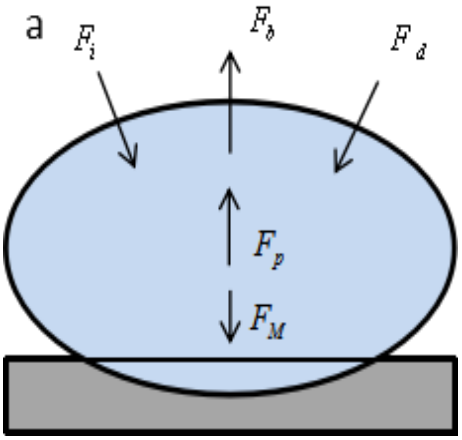
a
F_i
F_b
F_d
F_p
F_M

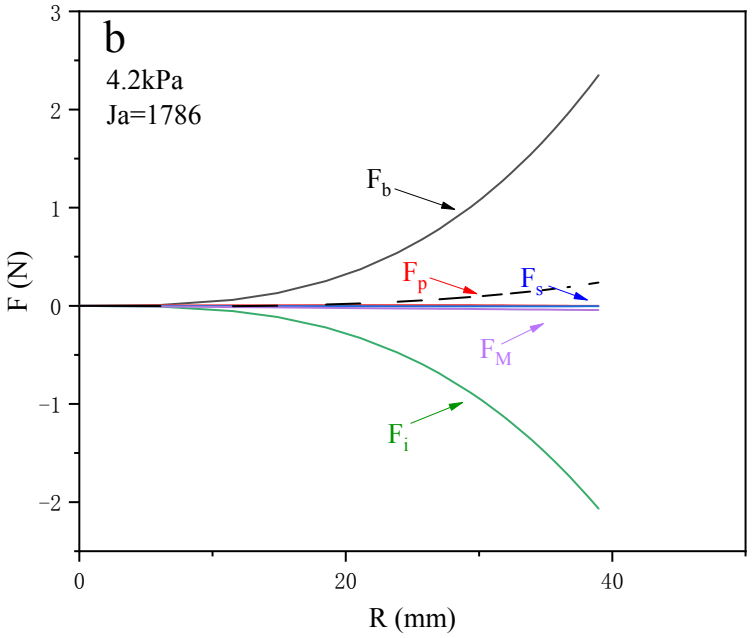
b
4.2kPa
Ja=1786
F_b
F_p
F_s
F_M
F_i
F (N)
R (mm)
3
2
1
0
−1
−2
0
20
40

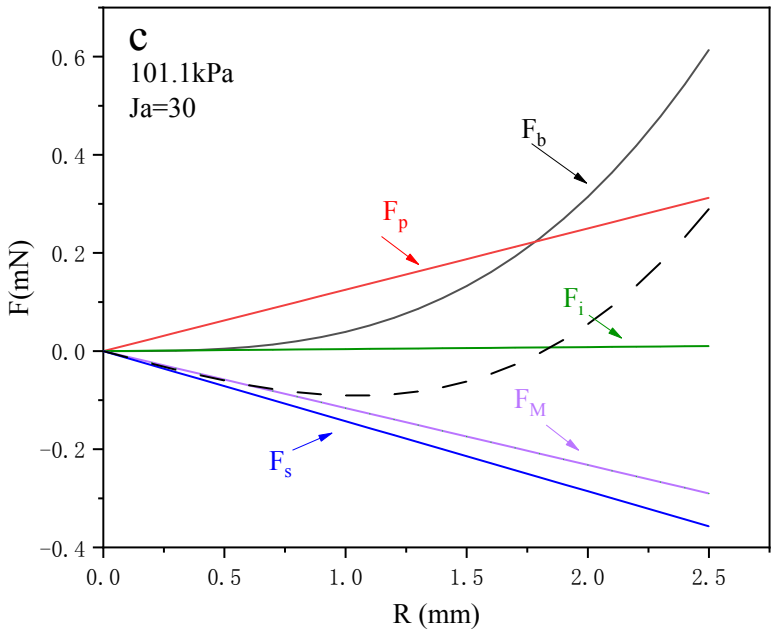

Figure.12. The geometric parameters and force acting on an isolated bubble(a)and the relationship between the forces acting on the isolated bubble and the bubble radius 4.2Kpa (b) 101.kPa(c)

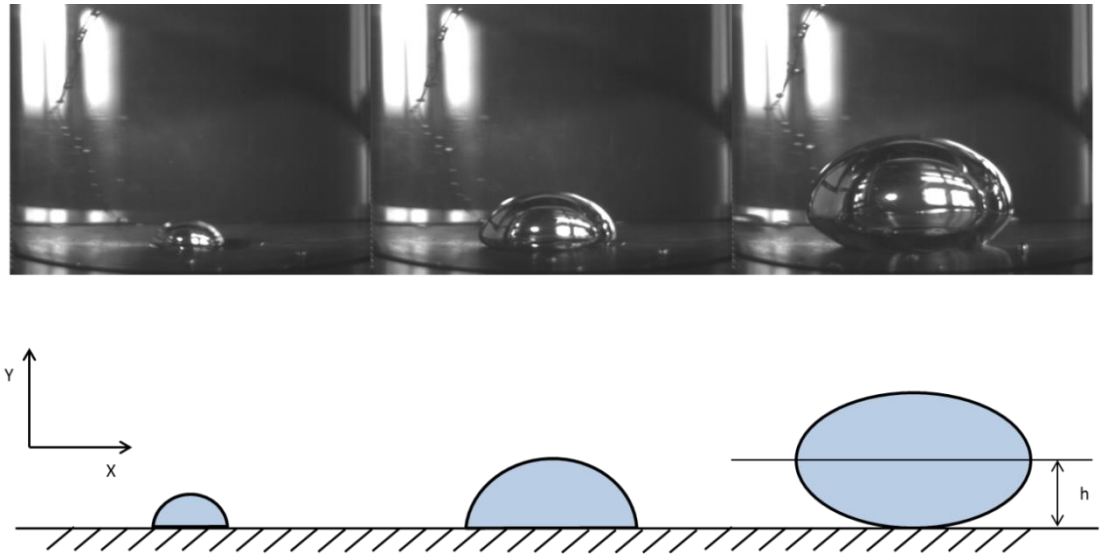

Figure.13. The growth and departure behavior of an isolated bubble under subatmospheric pressure

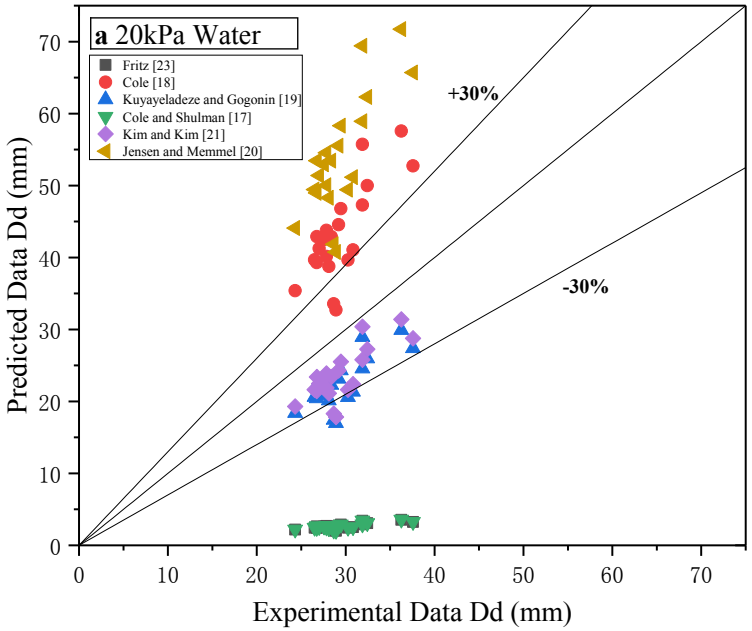
a 20kPa Water
Fritz [23]
Cole [18]
Kuyayeladeze and Gogonin [19]
Cole and Shulman [17]
Kim and Kim [21]
Jensen and Memmel [20]
+30%
-30%
Predicted Data Dd (mm)
Experimental Data Dd (mm)
0
10
20
30
40
50
60
70

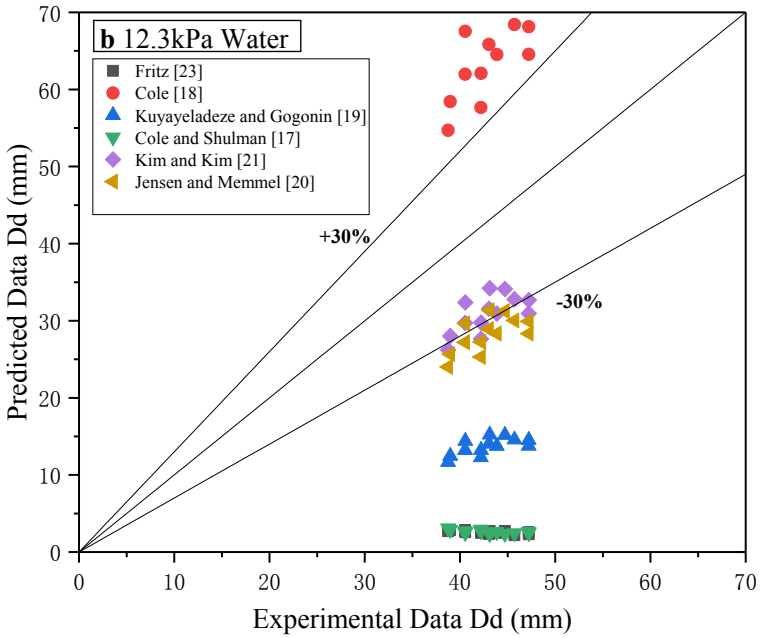
b 12.3kPa Water
Fritz [23]
Cole [18]
Kuyayeladeze and Gogonin [19]
Cole and Shulman [17]
Kim and Kim [21]
Jensen and Memmel [20]
+30%
-30%
Predicted Data Dd (mm)
Experimental Data Dd (mm)
0
10
20
30
40
50
60
70

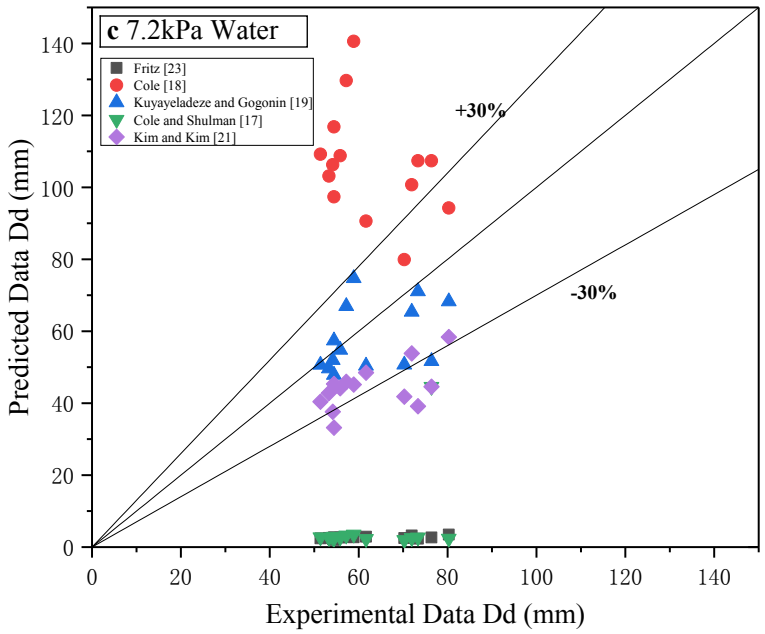
c 7.2kPa Water
Fritz [23]
Cole [18]
Kuyayeladeze and Gogonin [19]
Cole and Shulman [17]
Kim and Kim [21]
+30%
-30%
Predicted Data Dd (mm)
Experimental Data Dd (mm)
0
20
40
60
80
100
120
140

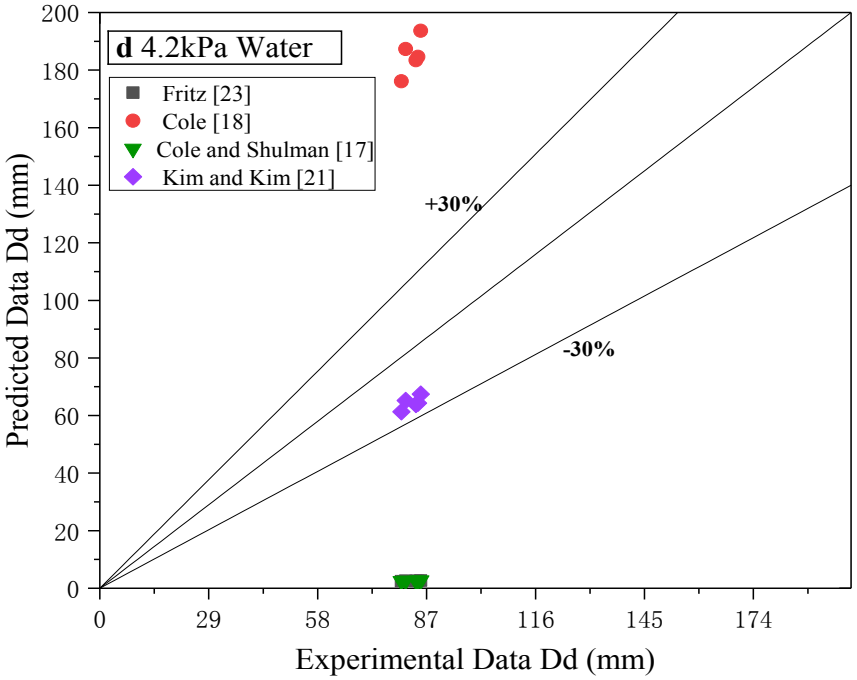
d 4.2kPa Water
Fritz [23]
Cole [18]
Cole and Shulman [17]
Kim and Kim [21]
+30%
-30%
Predicted Data Dd (mm)
Experimental Data Dd (mm)
0
20
40
60
80
100
120
140
160
180
200
0
29
58
87
116
145
174

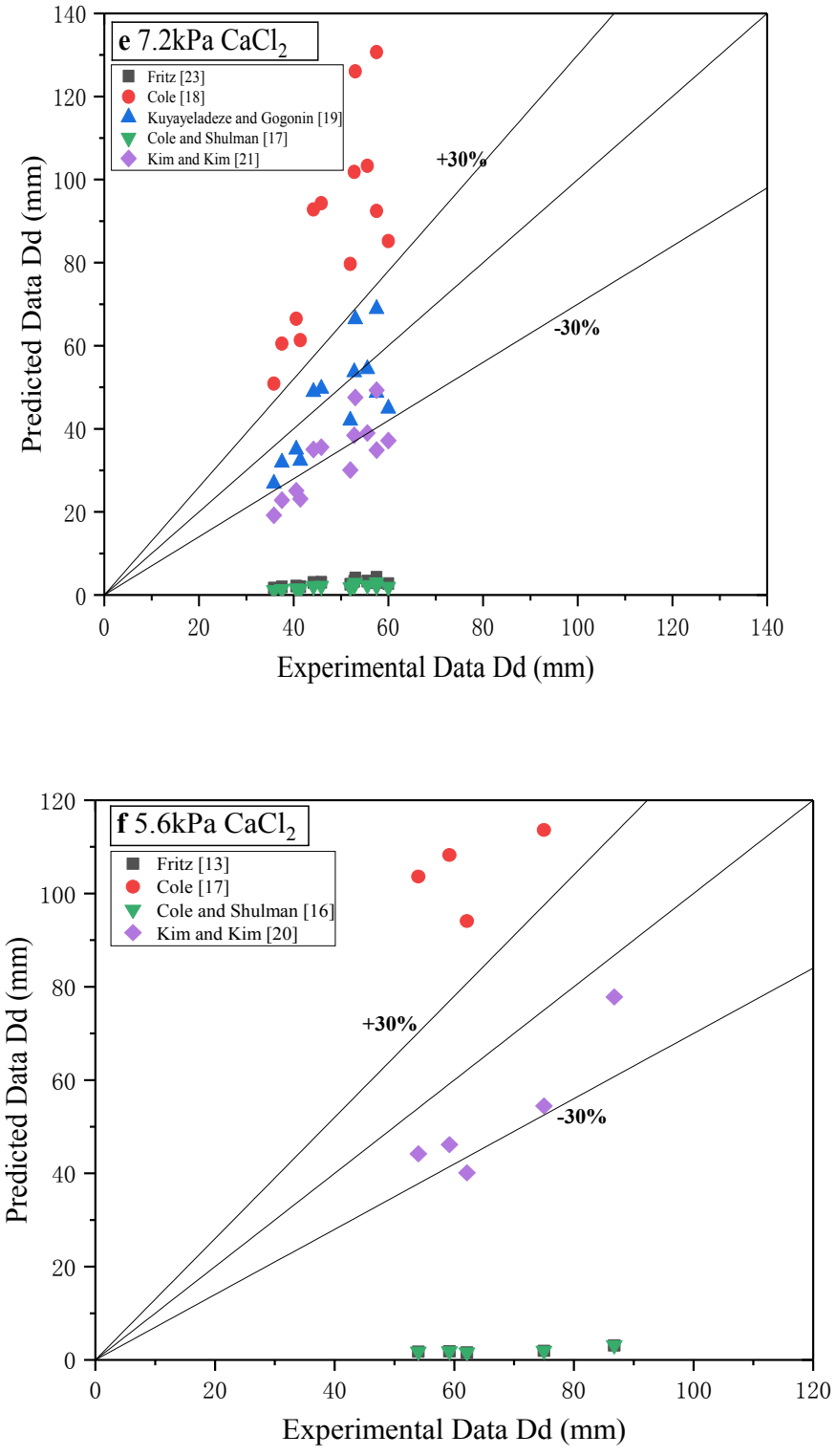

Figure.14. comparisons between the experimental and predicted bubble diameters with different correlations in different operating conditions

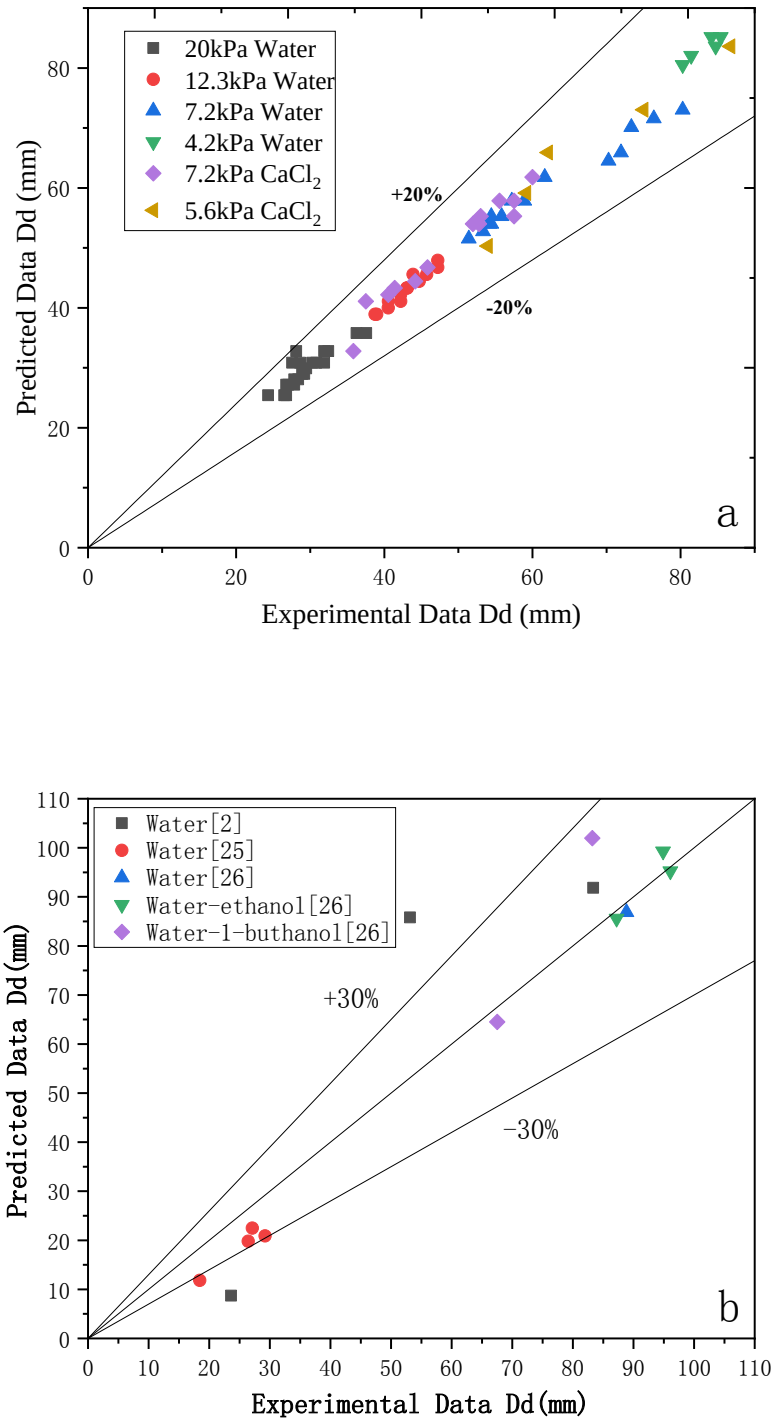

Figure.15. Comparisons between the experimental data and the new bubble departure diameter correlation in different operating conditions(a) and Comparisons of literature data and new bubble departure diameter correlation prediction data(b)

-able 1

Bubble departure diameter and frequency correlations

$D_d = 0.0208\theta[\frac{\sigma g_c}{g(\rho_l-\rho_v)}]^{1/2}\left[1+0.0025(\frac{dD}{dt})^{\frac{3}{2}}\right]$	Cole and Shulman[12]
$D_d = 0.04Ja[\frac{2\sigma}{g(\rho_l-\rho_v)}]^{1/2}$	Cole[13]
$D_d = 0.25(1+10^5K_1)^{1/2}[\frac{\sigma g_c}{g(\rho_l-\rho_v)}]^{1/2}$	Kutateladeze and Gogonon[14]
For $K_1 < 0.06$, where $K_1 = \left(\frac{Ja}{Pr_l}\right)^2 (Ar)^{-1}$	
$D_d = 0.19(1.8+10^5K_1)^{2/3}[\frac{\sigma}{g(\rho_l-\rho_v)}]^{1/2}$	Jensen and Memmel[15]
$D_d = 0.1649Ja^{0.7}[\frac{\sigma g_c}{g(\rho_l-\rho_v)}]^{1/2}$	Kim and Kim[16]

Table 2

Uncertainties of the measurement instruments and calculation

Parameter	Instrument	Uncertainty
Temperature (K)	K-type thermocouples	±0.1 K
Length (mm)	Ruler	±0.05mm
Pressure (kPa)	MD-GA-20K-1-P2-M9-A-T1 Absolute pressure transmitter	±0.2kPa
Heat Flux (W/cm^2)	Omega SA1-T-120	±8.2%
Wall temperature (K)		±0.1 K

Table 3

Operating parameter and physical properties

Wall Superheat	System Pressure	$CaCl_2$ Concentration
Range of operating parameter		
0 K – 40 K	3.6kPa – 22 kPa	15 wt% – 40 wt%

System Pressure	Water (101.3kPa)	Water (20kPa)	Water (4.2kPa)	$CaCl_2$ / Water (101.3kPa)
T_{sat} (℃)	100	60	30	103-110
σ (Nm^{-1})	0.05892	0.06023	0.07118	0.0785-0.0893
c_p ($Jkg^{-1}K^{-1}$)	4,236	4208	4175	2784-3342
K_1($Wm^{-1}k^{-1}$)	0.679	0.653	0.638	0.554-0.576
ρ_l (kgm^{-3})	958.4	978.2	998.5	1130-1286
ρ_V(kgm^{-3})	0.58	0.13	0.03	0.55

Table 4

The statistical analysis of the bubble departure diameter at subatmospheric pressures

Pressure (kPa)	Fluid	Correlations	AD	AAD
20	Water	Fritz [13]	-91.037	91.037
		Cole [18]	45.768	45.768
		Kuyayeladze and Gogonin [19]	-24.282	24.282
		Cole and Shulman [17]	-90.941	90.941
		Kim and Kim [21]	-20.513	20.513
		Jensen and Memmel [20]	82.414	82.414
12.3	Water	Fritz [13]	-93.963	93.963
		Cole [18]	50.891	50.891
		Kuyayeladze and Gogonin [19]	-67.833	67.833
		Cole and Shulman [17]	-93.893	93.893
		Kim and Kim [21]	-27.675	27.575
		Jensen and Memmel [20]	-33.768	33.768
7.2	Water	Fritz [13]	-95.812	95.812
		Cole [18]	68.910	68.910
		Kuyayeladze and Gogonin [19]	-18.706	18.706
		Cole and Shulman [17]	-95.751	95.751
		Kim and Kim [21]	-29.858	29.858

		Jensen and Memmel [20]	157.206	157.206
4.2	Water	Fritz [13]	-96.938	96.938
		Cole [18]	122.039	122.039
		Kuyayeladze and Gogonin [19]	/	/
		Cole and Shulman [17]	-96.933	96.933
		Kim and Kim [21]	-22.675	22.675
		Jensen and Memmel [20]	/	/
7.2	$CaCl_2$ Solution	Fritz [13]	-94.188	94.188
		Cole [18]	79.815	79.815
		Kuyayeladze and Gogonin [19]	-5.263	15.383
		Cole and Shulman [17]	-95.872	95.872
		Kim and Kim [21]	-28.15	32.15
		Jensen and Memmel [20]	192.63	192.63
5.6	$CaCl_2$ Solution	Fritz [13]	-97.063	97.063
		Cole [18]	73.54	73.54
		Kuyayeladze and Gogonin [19]	/	/
		Cole and Shulman [17]	-97.002	97.002
		Kim and Kim [21]	-28.34	38.34
		Jensen and Memmel [20]	/	/